Supplement of Atmos. Chem. Phys., 25, 2667–2694, 2025
https://doi.org/10.5194/acp-25-2667-2025-supplement

Atmospheric Chemistry and Physics
Open Access
EGU

Supplement of

Characterization of brown carbon absorption in different European environments through source contribution analysis

Hector Navarro-Barboza et al.

Correspondence to: Hector Navarro-Barboza (hector.navarro@bsc.es) and Oriol Jorba (oriol.jorba@bsc.es)

S1 Flowchart of the *k* optimization process

The optimization process described in Section 2.4 is illustrated in the flowchart shown in Figure S1. The procedure starts with the tagging of OA per source derived from MONARCH runs, followed by the application of a priori *k* values imposed based on Saleh (2020). The subsequent steps include calculating absorption and determining *k* values for each source with the SLSQP (Sequential Least Squares Programming) algorithm that minimizes the error with the observed absorption. The process concludes with the resulting optimized *k* values at 370 nm for each component and the calculation of the final OA absorption.

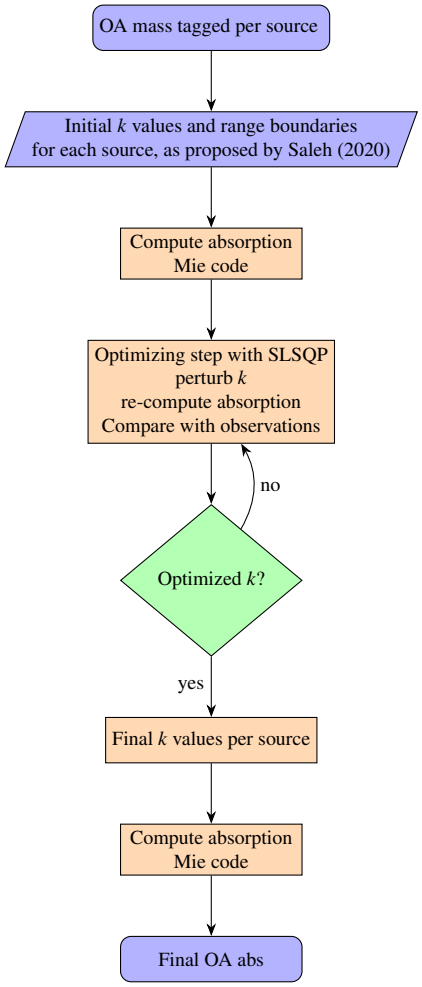

Figure S1. Steps to derive optimized imaginary refractive index *k* for total or tagged OA.

S2 Statistical metrics

The model results presented in Section 3 are evaluated using five statistical metrics: Normalized Mean Bias (NMB), Normalized Mean Error (NME), Pearson's correlation coefficient (r), Fraction of Predictions within a Factor of Two (FAC2) of observations and Fractional Bias (FB). We followed the performance assessment approach recommended by Emery et al. (2017) for photochemical models, particularly for pollutants such as Elemental Carbon (EC) and Organic Carbon (OC), fo-

cusing on metrics including FB, NME, and NMB. These recommendations are based on the "goal" and "criteria" proposed by Boylan and Russell (2006), where the "goal" signifies the peak performance expected from a model, and the "criteria" represent a level of performance that should be achievable by most models. The metrics are defined in Table S1.

Table S1. Statistical metrics used for model performance evaluation. m: model, o: observations.

Metric	Equation	Goal		Criteria	
		OC	EC	OC	EC
Normalized mean bias (NMB)	$\frac{\sum(m_i-o_i)}{\sum o_i} \times 100$	$< \pm 15\%$	$< \pm 20\%$	$< \pm 50\%$	$< \pm 40\%$
Normalized mean error (NME)	$\frac{\sum\lvert m_i-o_i\rvert}{\sum o_i} \times 100$	$< 45\%$	$< 50\%$	$< 65\%$	$< 75\%$
Fractional bias (FB)	$\frac{2}{N}\sum\frac{(m_i-o_i)}{(o_i+o_i)}$	$< \pm 30\%$[a]	$< \pm 30\%$[a]	$< \pm 60\%$[a]	$< \pm 60\%$[a]
Factor two (FAC2)	Fraction where $0.5 < m/o < 2$	–	–	$\geq \pm 50\%$[b]	$\geq \pm 50\%$[b]
Pearson correlation coefficient (r)	$\frac{\sum[(m_i-\overline{m})\times(o_i-\overline{o})]}{\sqrt{\sum(m_i-\overline{m})^2\times\sum(o_i+\overline{o})^2}}$	–	–	–	–
Bias	$\frac{\sum(m_i-o_i)}{N}$	–	–	–	–
Root mean square error (RMSE)	$\sqrt{\frac{1}{N}\sum(m_i-o_i)^2}$	–	–	–	–

[a] Recommended FB values for PM by Boylan and Russell (2006).

[b] Recommended metrics for air quality models by Chang and Hanna (2004) and Soni et al. (2021).

S3 Evaluation of OA Concentrations Across Europe

Figure S2 presents scatter plots comparing modeled and observed OA concentrations at the 12 stations. The correlation coefficients (r) vary by site, ranging from 0.21 at MSY to 0.77 at PAY, indicating different levels of agreement between the model and observations. At the KRA and DEM stations, the model tends to overestimate OA concentrations, as indicated by positive fractional bias (FB) values of 32.17 and 34.57, respectively. Conversely, at the HEL and MSY stations, the model underestimates OA concentrations, with negative FB values of -19.31 and -37.90, respectively. Seasonal variations are evident in the scatter plots. Higher concentrations are observed during the DJF (blue) and MAM (orange) seasons, particularly at KRA and RIG, while lower concentrations are seen during the JJA (green) and SON (red) seasons. This seasonal trend highlights the importance of considering temporal variations in OA modeling.

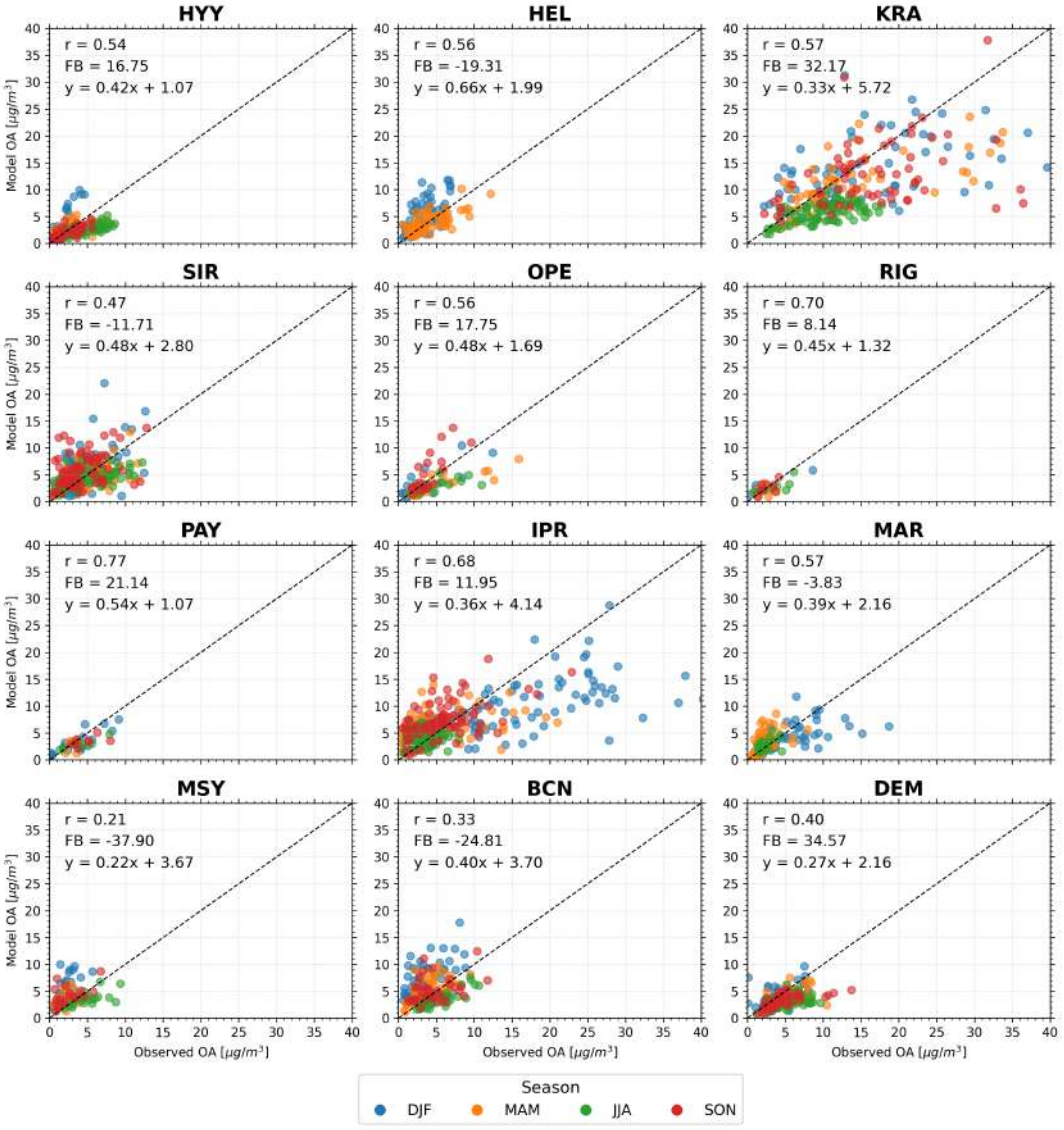

Figure S2. Scatter plots comparing modeled and observed OA concentrations across twelve different locations (HYY, HEL, KRA, SIR, OPE, RIG, PAY, IPR, MAR, MSY, BCN, DEM). Each plot includes data points color-coded by season: DJF (blue), MAM (orange), JJA (green), and SON (red). The plots also display the correlation coefficient (r), fractional bias (FB), and the linear regression equation (y) for each location. The dashed line represents the 1:1 line, indicating perfect agreement between modeled and observed values.

Complementary, Table S2 summarizes the statistical evaluation of the 12 stations (DJF December-January-February; MAM March-April-May; JJA June-July-August; SON September-October-November). In general, the "criteria" are met in most stations and seasons, although some sites fall short of the more stringent "goal". A key trend observed is that the model performs most robustly during the spring season (MAM), with many stations reaching the "goal" and "criteria". In contrast, the summer (JJA) and winter (DJF) seasons exhibit greater variability.

During winter (DJF), several stations show strong correlations, such as HYY ($r = 0.9$), but discrepancies arise in metrics such as FAC2 (e.g., HYY with a low $FAC2 = 23.5$), indicating a tendency to overestimate OA concentrations during this period. This overestimation is likely related to the representation of residential emissions in the model, which are dominant

during the colder months. In contrast, during the spring season (MAM) shows improved model performance, particularly at stations such as HEL, were high FAC2 value (93.6%) and strong correlation ($r = 0.7$) suggest a better balance between emission sources and atmospheric processes during this period. Fire emissions, which increase in significance during spring, may contribute to improved accuracy (Urbieta et al., 2015; Turco et al., 2017). Many stations show their best performance during MAM, achieving low FB and NME, such as SIR, which demonstrates consistent accuracy across multiple metrics.

Summer (JJA) and autumn (SON) introduce greater variability in model performance. Some stations, such as KRA in SON, exhibit low correlations ($r = 0.3$), but others maintain high FAC2 values, like PAY in JJA (100%) and RIG in SON (100%). This suggests that, while the model effectively captures overall concentrations in some cases, it faces difficulties with temporal dynamics, particularly the biogenic SOA contributions that become more pronounced during the warmer months. The challenges of modeling biogenic SOA during JJA are particularly evident at stations such as HYY and MSY, where the model underestimates the observed peaks in OA concentrations, driven by SOA formation. Stations like SIR and OPE manage to meet NME and NMB targets in these seasons, despite challenges in FB, as highlighted in gray in Table S2.

Data availability varies across stations, with notable gaps at HEL and MAR during JJA and SON, which limits the ability to fully assess model performance at these locations for those periods. Overall, the analysis indicates that while the model performs well across seasons, particularly in spring, it faces challenges during summer and winter in fully capturing the complex processes driving OA concentrations. These limitations are especially evident in modeling residential emissions during winter and SOA formation in summer.

Table S2. Seasonal statistical evaluation of OA concentrations. Goal achievement (Gray) and criteria benchmarks (Bold) based on Emery et al. (2017). NMB: Normalized Mean Bias, NME: Normalized Mean Error, and FAC2 expressed as percentages.

Metric	r	FAC2	FB	NME	NMB	r	FAC2	FB	NME	NMB	r	FAC2	FB	NME	NMB	r	FAC2	FB	NME	NMB
Season	DJF	DJF	DJF	DJF	DJF	MAM	MAM	MAM	MAM	MAM	JJA	JJA	JJA	JJA	JJA	SON	SON	SON	SON	SON
STN																				
HYY	0.94	23.53	84.43	146.11	146.11	0.64	**79.17**	**-9.02**	**45.37**	**-8.63**	0.84	**73.56**	**-52.56**	**43.73**	**-41.62**	0.83	**72.13**	**-3.78**	**39.10**	**-3.71**
HEL	0.65	**66.10**	**45.89**	70.61	59.55	0.72	**93.59**	**-3.64**	**33.46**	**-3.58**	nan	nan	nan	nan	nan	nan	nan	nan	nan	nan
KRA	0.53	**73.33**	**-26.97**	**44.80**	**-23.77**	0.67	**90.48**	**-20.53**	**32.72**	**-18.62**	0.55	**65.43**	**-55.38**	**44.73**	**-43.37**	0.34	**74.63**	**-32.54**	**41.06**	**-27.99**
SIR	0.61	**61.84**	**28.93**	**58.73**	**33.82**	0.55	**79.27**	**-3.06**	**37.00**	**-3.02**	0.63	**87.78**	**-12.93**	**38.48**	**-12.14**	0.36	**66.25**	**32.90**	**64.81**	**39.37**
OPE	0.80	**70.59**	**-4.48**	**45.92**	**-4.38**	0.85	**68.42**	**-52.85**	**43.28**	**-41.81**	0.57	**66.67**	**-51.30**	**43.48**	**-40.83**	0.78	**85.00**	**29.82**	**49.58**	**35.05**
RIG	0.94	40.00	**10.77**	**53.95**	**11.38**	-0.06	**71.43**	**-14.61**	**50.09**	**-13.62**	0.77	**75.00**	**-24.56**	**32.22**	**-21.88**	0.61	**100.00**	**3.16**	**26.98**	**3.21**
PAY	0.84	**76.47**	**-12.39**	**32.32**	**-11.67**	0.09	**85.71**	**-13.43**	**28.80**	**-12.58**	0.86	**100.00**	**-32.95**	**33.78**	**-28.29**	0.51	**87.50**	**-31.94**	**29.23**	**-27.54**
IPR	0.62	**61.54**	**-50.53**	**43.89**	**-40.34**	0.33	49.32	**17.31**	70.19	**18.95**	0.26	**75.28**	**17.77**	**45.24**	**19.50**	0.52	**71.43**	**21.84**	**52.85**	**24.51**
MAR	0.61	**80.77**	**-29.05**	**37.95**	**-25.36**	0.49	**77.78**	**38.48**	**63.81**	**47.64**	0.48	**96.00**	**15.29**	**33.37**	**16.56**	nan	nan	nan	nan	nan
MSY	0.66	14.29	95.00	180.93	180.93	0.39	**57.14**	**54.86**	86.62	75.59	0.63	**86.96**	**-31.59**	**29.38**	**-27.28**	0.52	**70.00**	**48.39**	69.02	63.84
BCN	0.58	41.82	70.13	112.18	108.01	0.62	**80.00**	**28.34**	**44.92**	**33.02**	0.80	**86.96**	**-37.33**	**32.21**	**-31.46**	0.37	**75.00**	**13.24**	**45.74**	**14.17**
DEM	0.47	**83.33**	**-0.40**	**36.28**	**-0.40**	0.41	**86.21**	**-38.31**	**35.59**	**-32.15**	0.38	**72.22**	**-50.43**	**42.66**	**-40.27**	0.58	**83.02**	**-32.00**	**30.10**	**-27.59**

S4 OA concentrations and source contribution at BCN and MSY sites using a local bottom-up emission inventory

Figure S3 shows the time series of OA concentrations and source contributions for BCN and MSY sites derived from a simulation of the MONARCH model using a local bottom-up emission inventory for Spain (HERMESV3_BU; Guevara et al., 2020). The simulation was conducted for the months of January and July with a spatial resolution of $\sim$ 5 km. The main differences between HERMESv3_BU and CAMS-REG_v4.2 inventories are discussed in Navarro-Barboza et al. (2024). In contrast to results using the CAMS inventory depicted in Figure 3, results with the HERMESv3_BU inventory closely align with observational data in BCN and MSY, particularly during winter. The comparison between the two inventories reveals marked differences in OA component contributions. For instance, with HERMESv3_BU, the residential component is less dominant than with CAMS, and the traffic component becomes more significant. A similar pattern is observed in MSY, where the CAMS inventory results tend to overestimate winter concentrations due to the residential component. These discrepancies highlight the existing constraints of European-scale emission inventories, although they remain the most reliable information source at present.

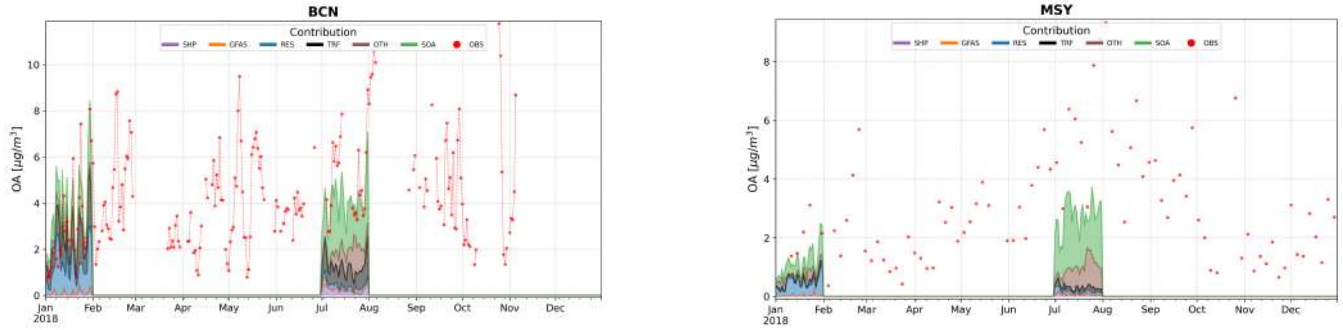

(a) (b)

Figure S3. Daily average contributions of OA concentration in BCN (a) and MSY (b) for the year 2018, using the local bottom-up HERMESv3 emission inventory. Measurements are expressed in [$\mu\ gm^{-3}$], with each component distinguished by a specific color: Shipping (SHIP) in purple, Fires (GFAS) in orange, Residential (RESI) in blue, Traffic (TRAF) in black, Other (OTHR) in brown, and Secondary OA (SOA) in green. Observational data (OBS) are marked with red dots. Due to the limitations in simulation data availability, only the months of January and July are depicted.

S5 *k* optimization results

The results of the performed *k* optimization process are summarized in Table S3, which presents the mean and standard deviation (std) of obtained *k* values across stations, classified by representative environments (Regional - REG, Suburban - SUB, Urban - URB; see Table 1), and optimization cases 1 through 4 (Table 3). Each case corresponding to unique assumptions discussed in Sect. 2.5. The mean *k* and std were analyzed for the five sources of study: GFAS, RESI, SHIP, TRAF, and OTHR. The row labeled "ALL" indicates the average values for all stations in Case 4.

Overall, for all settings and cases (1-4), and also for ALL, the highest *k* was obtained for GFAS compared to the other sources with the highest *k* observed for URB sites, whereas similar *k* within the std were obtained at REG and SUB sites. In each setting, small differences were observed between Case 1 (GFAS weakly) and Cases 2 and 4 (GFAS moderately) indicating a robust estimation of GFAS *k* in-between weakly and moderately absorbing OA. Interestingly, in Case 3 (GFAS strongly) *k* reached the lowest allowed limit (cf. Table 3) with zero std (cf. Table S3) suggesting that GFAS OA cannot be treated as strongly absorbing.

RESI OA were considered as weakly absorbing (Cases 1 and 4) and moderately absorbing (Cases 2 and 3). Similarly to GFAS, higher RESI *k* was obtained for URB sites even if for this source the obtained *k* were comparable, within the std, among the three considered settings. This similarity could be associated with the fact that RESI emissions are mostly local, thus reducing the differences between the station settings. Moreover, for each setting small differences were observed for RESI *k* among the 4 considered Cases suggesting a robust estimation of the RESI *k* that lied in-between weakly and moderately absorbing OA. Note that for both GFAS and RESI the optimization process provided *k* values closer to the upper limit of the weakly category rather than the upper limit of the category moderately.

Similarly to RESI, SHIP emissions were considered weakly absorbing in Cases 1 and 4, and moderately absorbing in Cases 2 and 3. Overall, the optimization process provided rather similar *k* among the four Cases at URB sites with *k* values that were higher compared to REG and SUB. At URB sites, the SHIP *k* lied in-between the categories weakly and moderately with *k* values that, as for GFAS and RESI, were closer to the lower limit of the category moderately. At SUB sites, the SHIP *k* reached the lowest limit allowed for the category weak (0.005; Cases 1 and 4) and moderately (0.02; Cases 2 and 3) suggesting very low *k* of SHIP for this setting. At REG sites, SHIP *k* was higher than at SUB sites with low variability among Cases 1, 2 and 4 and higher values and much higher std for case 3. Also for REG sites the optimization process suggest that SHIP OA emissions were more weakly absorbing than moderately absorbing.

TRAF emissions were treated as very weakly absorbing in Cases 1, 2 and 3 and as weakly absorbing in Case 4. Interestingly, the highest TRAF *k* were obtained for URB sites whereas much lower *k* were obtained at REG and SUB sites. At URB sites,

Cases 1, 2 and 3 provided k values in the upper range of the very weakly category (0.04; cf. Table 3) with very low std suggesting that TRAF emissions were weakly absorbing rather than very weakly absorbing. In fact, Case 4 provided a TRAF k value of 0.06 that lied in-between the lower and upper limit of the category weakly absorbing. At both SUB and REG sites, the obtained TRAF k values were much lower compared to URB sites. This result is consistent with recent evidence that OA from traffic in urban sites can be an important source of brown OA (e.g., Ho et al., 2023). Moreover, traffic emissions are not expected to be primarily local at REG and SUB sites, thus likely contributing to the observed reduced TRAF k in these two settings due to physico-chemical OA processes as dilution and photobleaching.

OTHR emissions were treated as very weakly absorbing for all the considered cases (1-4). The optimization process provided very low k values confirming the very low absorption properties of OA particles emitted by OTHR sources. Note that higher OTHR k values were obtained at URB sites compared to REG and SUB sites where the obtained k were very close to the lower k value in the category very weakly (cf. Table 3).

Table S3. Statistical summary of mean and standard deviation (std) values for the optimization of the imaginary refractive index across the three settings (REG, SUB, URB) and the four cases (Case 1, Case 2, Case 3, Case 4). Each case corresponds to different assumptions detailed in Table 3, analyzed across five OA sources: GFAS, RESI, SHIP, TRAF, and OTHR. The row labeled "ALL" represents the averaged values across all stations for Case 4.

		GFAS		RESI		SHIP		TRAF		OTHR	
	Metric	mean	std	mean	std	mean	std	mean	std	mean	std
Setting	Case										
REG	Case 1	0.0619	0.0396	0.0458	0.0469	0.0196	0.0168	0.0093	0.0141	0.0015	0.0009
	Case 2	0.0506	0.0434	0.0482	0.0448	0.0210	0.0071	0.0070	0.0139	0.0018	0.0010
	Case 3	0.1241	0.0053	0.0476	0.0447	0.0527	0.0536	0.0068	0.0140	0.0014	0.0005
	Case 4	0.0615	0.0387	0.0451	0.0462	0.0182	0.0150	0.0122	0.0132	0.0014	0.0008
SUB	Case 1	0.0409	0.0154	0.0409	0.0154	0.0049	0.0000	0.0011	0.0000	0.0014	0.0005
	Case 2	0.0403	0.0148	0.0403	0.0148	0.0191	0.0017	0.0011	0.0000	0.0013	0.0003
	Case 3	0.1219	0.0000	0.0395	0.0135	0.0181	0.0000	0.0011	0.0000	0.0011	0.0000
	Case 4	0.0398	0.0146	0.0398	0.0146	0.0049	0.0000	0.0049	0.0000	0.0012	0.0001
URB	Case 1	0.0924	0.0354	0.0635	0.0535	0.0418	0.0481	0.0354	0.0000	0.0098	0.0109
	Case 2	0.0998	0.0238	0.0635	0.0534	0.0445	0.0456	0.0354	0.0000	0.0092	0.0102
	Case 3	0.1229	0.0017	0.0634	0.0535	0.0527	0.0599	0.0345	0.0015	0.0091	0.0110
	Case 4	0.0934	0.0291	0.0625	0.0551	0.0314	0.0458	0.0579	0.0078	0.0081	0.0105
ALL	Case 4	0.0640	0.0342	0.0481	0.0388	0.0182	0.0231	0.0218	0.0229	0.0030	0.0052

S6 Evaluation of absorption results employing different optimized *k* values

Figure S4 shows a scatter plot of the observed versus modeled OA absorption at each monitoring site. The plot uses results from Case 4 (all) and Case 5 (all), where k values were obtained using all the monitoring stations combined. To calculate total absorption, Case 4 uses individual k values tailored to specific OA components: 0.0571 for fires, 0.0403 for RESI, 0.0571 for SHIP, 0.0049 for TRAF, and 0.0011 for OTHR. Meanwhile, Case 5 applies a single k value of 0.0187 across all sources. The key difference between the cases is that Case 4 includes a detailed source apportionment, discerning five different OA sources, while Case 5 considers the total OA without source differentiation. Complementary, Figure S5 shows similar results to Figure S4, but using k values optimized for each individual monitoring site (by stn). The statistics and time series for the latter case are presented in Table S4 and Figure S6, respectively.

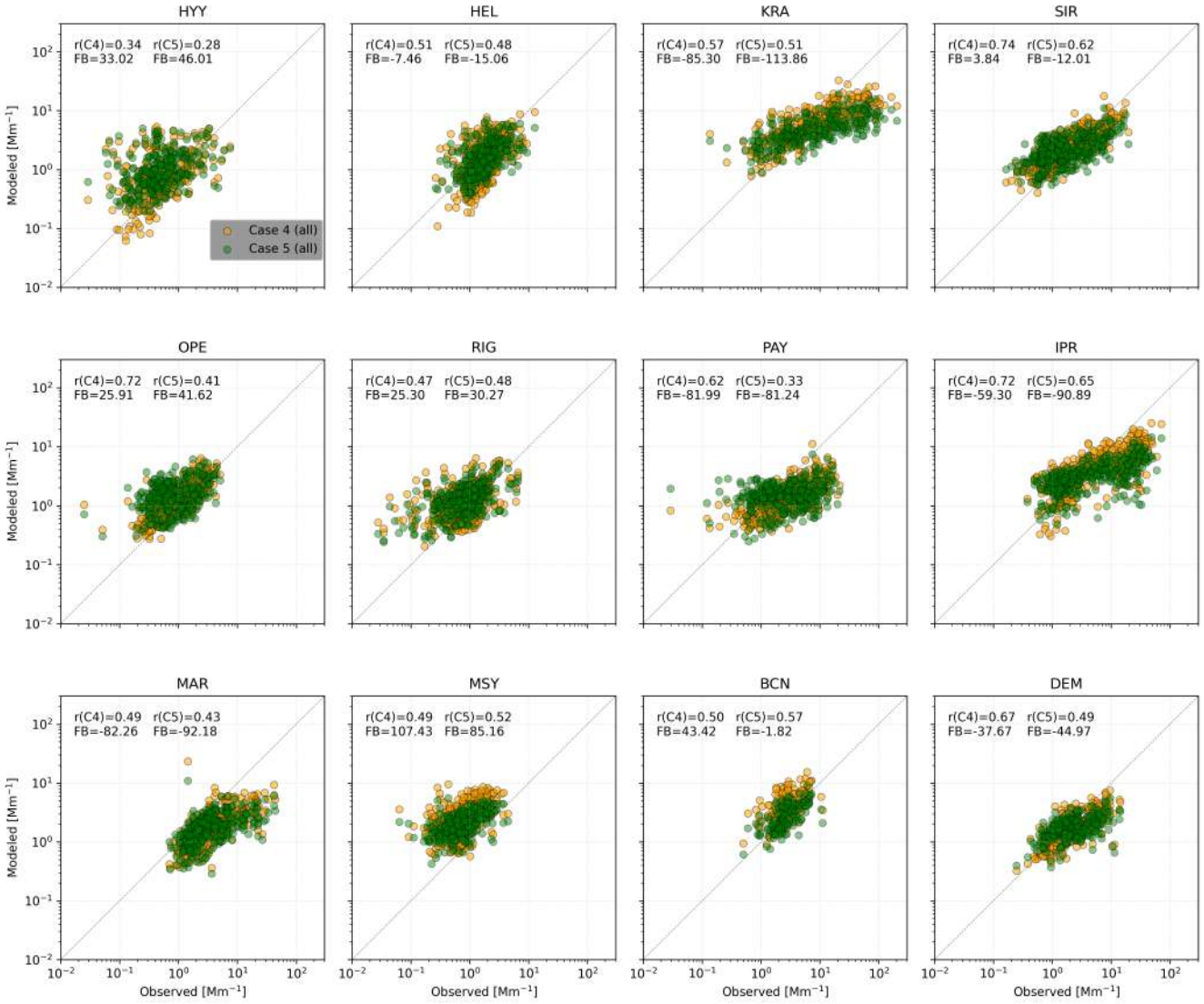

Figure S4. Daily mean observed versus modeled OA absorption for Case 4 (all) and Case 5 (all) scenarios, with the imaginary refractive index (k) values derived from aggregated data across all monitoring stations. Each panel includes the correlation coefficients (r) and fractional bias (FB).

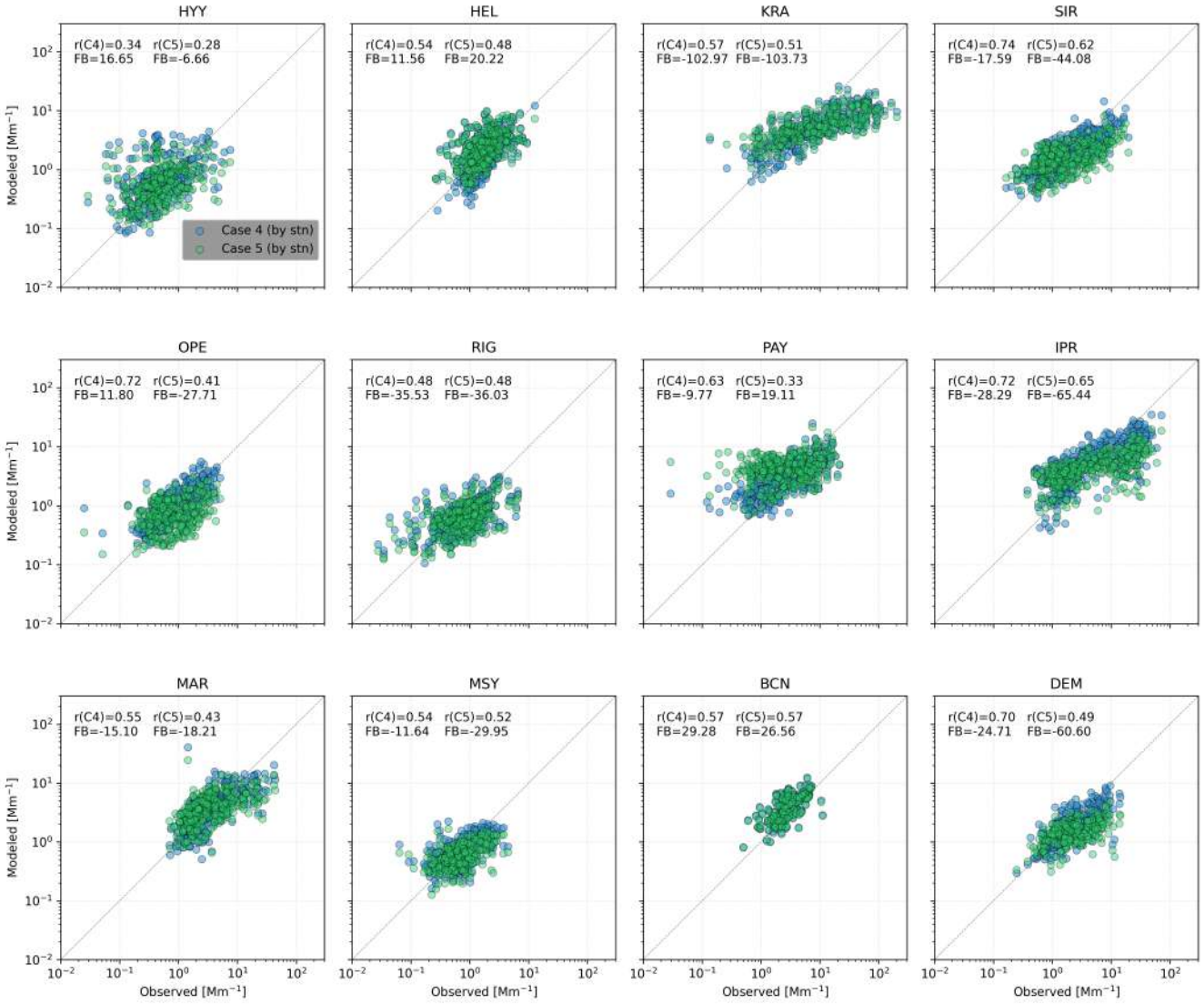

Figure S5. Similar to Figure S4, but with k derived for each station.

Table S4. Statistical evaluation of absorption results for Cases 4 and 5 by stn.

Cases		Case 4			Case 5	
Metric	r	FB	FAC2	r	FB	FAC2
HYY	0.34	16.65	63.96	0.28	-6.66	58.66
HEL	0.54	11.56	74.79	0.48	20.22	78.08
KRA	0.57	-102.97	48.92	0.51	-103.73	43.17
SIR	0.74	-17.59	71.07	0.62	-44.08	56.75
OPE	0.72	11.80	80.58	0.41	-27.71	56.31
RIG	0.48	-35.53	67.04	0.48	-36.03	67.32
PAY	0.63	-9.77	68.77	0.33	19.11	44.11
IPR	0.72	-28.29	54.40	0.65	-65.44	43.13
MAR	0.55	-15.10	79.32	0.43	-18.21	65.16
MSY	0.54	-11.64	78.63	0.52	-29.95	80.34
BCN	0.57	29.28	77.94	0.57	26.56	80.88
DEM	0.70	-24.71	84.45	0.49	-60.60	62.54

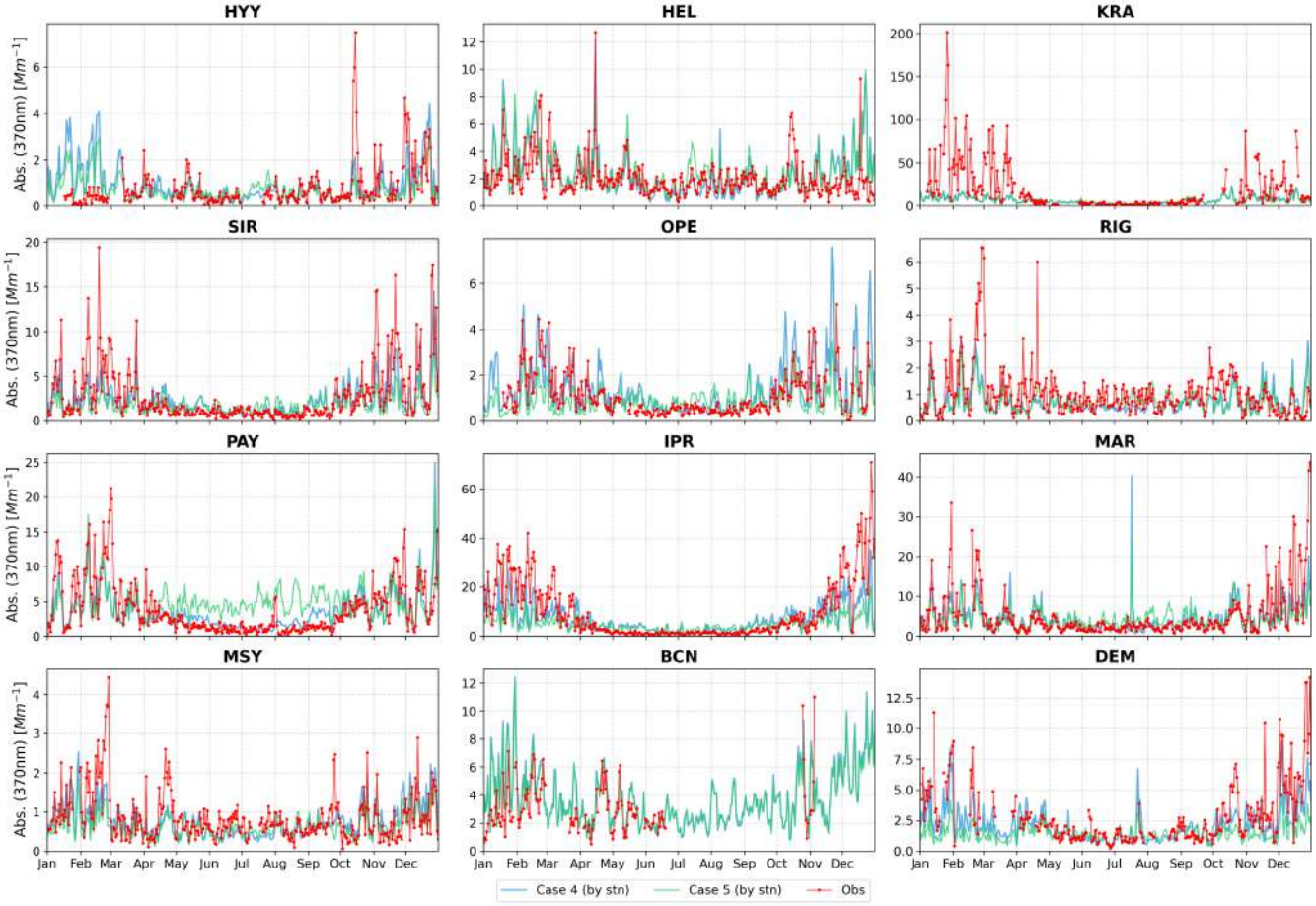

Figure S6. OA light absorption (370 nm) time series for 12 sites. Observed (Obs) in red and modeled absorption for Case 4 (by stn) (blue line) and Case 5 (by stn) (green line). *k* values derived at eact station.

References

Boylan, J. W. and Russell, A. G.: PM and light extinction model performance metrics, goals, and criteria for three-dimensional air quality models, Atmospheric environment, 40, 4946–4959, 2006.

Chang, J. C. and Hanna, S. R.: Air quality model performance evaluation, Meteorology and Atmospheric Physics, 87, 167–196, 2004.

Emery, C., Liu, Z., Russell, A. G., Odman, M. T., Yarwood, G., and Kumar, N.: Recommendations on statistics and benchmarks to assess photochemical model performance, Journal of the Air & Waste Management Association, 67, 582–598, 2017.

Guevara, M., Tena, C., Porquet, M., Jorba, O., and Pérez García-Pando, C.: HERMESv3, a stand-alone multi-scale atmospheric emission modelling framework–Part 2: The bottom–up module, Geoscientific Model Development (GMD), 13, 873–903, 2020.

Ho, C. S., Lv, Z., Peng, J., Zhang, J., Choe, T.-H., Zhang, Q., Du, Z., and Mao, H.: Optical properties of vehicular brown carbon emissions: Road tunnel and chassis dynamometer tests, Environmental Pollution, 320, 121 037, 2023.

Navarro-Barboza, H., Pandolfi, M., Guevara, M., Enciso, S., Tena, C., Via, M., Yus-Díez, J., Reche, C., Pérez, N., Alastuey, A., et al.: Uncertainties in source allocation of carbonaceous aerosols in a Mediterranean region, Environment international, 183, 108 252, 2024.

Saleh, R.: From measurements to models: toward accurate representation of brown carbon in climate calculations, Current Pollution Reports, 6, 90–104, 2020.

Soni, A., Mandariya, A. K., Rajeev, P., Izhar, S., Singh, G. K., Choudhary, V., Qadri, A. M., Gupta, A. D., Singh, A. K., and Gupta, T.: Multiple site ground-based evaluation of carbonaceous aerosol mass concentrations retrieved from CAMS and MERRA-2 over the Indo-Gangetic Plain, Environmental Science: Atmospheres, 1, 577–590, 2021.

Turco, M., von Hardenberg, J., AghaKouchak, A., Llasat, M. C., Provenzale, A., and Trigo, R. M.: On the key role of droughts in the dynamics of summer fires in Mediterranean Europe, Scientific reports, 7, 81, 2017.

Urbieta, I. R., Zavala, G., Bedia, J., Gutiérrez, J. M., San Miguel-Ayanz, J., Camia, A., Keeley, J. E., and Moreno, J. M.: Fire activity as a function of fire–weather seasonal severity and antecedent climate across spatial scales in southern Europe and Pacific western USA, Environmental Research Letters, 10, 114 013, 2015.